Hypersonic Flow Computations by Using An Equivalent Gas Model

S. Shitrit[a] and E. Arad[b]
Aeronoutical Systems, RAFAEL Advanced Defense Systems LTD., Israel

The aerodynamic of hypersonic vehicles is highly affected by enthalpy or "real gas" effects. It is the purpose of the current study, to assess the proper formulation of computational fluid dynamics required for simulation of high enthalpy flows. Under the assumption of chemical and thermal equilibrium , a functional representation have been employed for specific heat at constant pressure, thermal conductivity and viscosity coefficients for air at 500 to $30000\,K$ and pressure range of 10^{-4} to 100 atm. The proposed approach is evaluated using three test cases: HB-2, blunt cone and blunt double cone configurations at hypersonic flow. It is shown that the equivalent gas model is capable of capturing the main features of these flow fields and compares well with experiments.

[a] shlomis1@rafael.co.il
[b] eran@rafael.co.il

Nomenclature

(Nomenclature entries should have the units identified)

$A_{C_p}, B_{C_p}, C_{C_p}, D_{C_p}, E_{C_p}$ = curve-fit coefficients for specific heat at constant pressure C_p

$A_\mu, B_\mu, C_\mu, D_\mu, E_\mu, F_\mu$ = curve-fit coefficients for viscosity μ

A_K, B_K, C_K, D_K, E_K = curve-fit coefficients for total thermal conductivity K

α = acceleration, m/s^2

C_i = mass fraction of species i

C_p = total specific heat at constant pressure

Δx = variable displacement vector

f = residual value vector

F = force, N

h = enthalpy

h_i = enthalpy of species i

h_{tot} = total enthalpy

J = jacobian matrix

K = thermal conductivity

m = mass, kg

μ = molecular viscosity

NS = number of species

p = static pressure

Pr = prandtl number

p_{tot} = total pressure

R = gas constant

ρ = density, g/cm^3

ρ_i = density of species i, g/cm^3

T = static temperature

x = variable value vector

Z = compressibility factor

Subscript

i = Variable number

tot = Total values

I. Introduction

Numerical simulation of fluid flow is currently an integral part in the design process of a flight vehicle. The extreme conditions experienced in hypersonic flight are difficult to reproduce in an experimental facility. The cost of such hypersonic experimental studies is higher than low speed flow because of the immense amount of energy that is required to reproduce the flight conditions. Furthermore, the number of facilities which are equiped and capabale to perform such experiments, is very limited. The Computational Fluid Dynamics (CFD) application can reduce the number of costly experiments by providing deep insight into the flow field.

The high speed of hypersonic flows causes many physical phenomena that are not modeled by the common perfect gas form of the Navier-Stokes equations. Such particular phenomena include caloric and chemical effects, additional aerodynamic forces, plasma effects, thermal and chemical non-equilibrium and ionization [1]. In order to simulate these phenomena and describe the flow physics, the use of a real gas model is required. Therefore, instead of the single global continuity equation, a number of species continuity equations should employed as the number of species that may be present within the flow field. In this setup it is possible to track of the creation and destruction of species. In addition, a conservation equation for vibrational energy is also needed. To accurately describe the chemical reactions and energy mode relaxations, source terms need to be introduced which do not exist in the perfect gas formulation. Furthermore, additional terms need to be included in the energy and continuity equations to account for diffusion within the flow. As the numerical modeling improved and computer power increased, some methods were developed, which allow the simulation of the full Navier-Stokes equations for general geometries at these demanding flow conditions [2]. A pioneering computation of multidimensional flow-field including thermo-chemical non-equilibrium and ionization was performed by Candler [3] who solved a set of equations that coupled thermal and chemical non-equilibrium equations to the fluid dynamic equations. Another CFD code for entry flows called LAURA (Langley Aerothermodynamic Upwind Relaxation Algorithm) was developed by Gnoffo [4] at NASA Langely Research center. This code solves set of equations developed by Lee [5]. However, such a complicated codes and flow field calculations based on either of these approaches

(or similar) are characterized by reduced computational efficiency. Simplification can be obtained by assuming a chemical equilibrium without elemental separation. This allows the governing equations to be written in a functional form, so that the specific heat at constant pressure, Cp, thermal conductivity, K, and molecular viscosity, μ, are defined as total properties. Meaning that the energy equation do not contain the species production rate term apearing in the viscous-shock-layer form of the energy equation for a chemically reacting multicomponent gas mixture. As a result,the energy equation has the same form as the perfect gas equations. That way the equations for an equilibrium reacting gas mixture can be solved in a manner similar to that of a perfect gas [6].

The current study focuses on the implementation of an Equivalent Gas Model (EGM) for weakly ionized hypersonic flows in thermo-chemical equilibrium into compressible flow solver around complex configurations.

The derivation presented here of the EGM is based on the 11-species air model published by Gupta [6]. This report presents an accurate curve fits for the computed values of enthalpy, total specific heat, compressibility factor, viscosity, and total values of thermal conductivity and Prandtl number, for equilibrium air from 500 to $30000\,K$ over a pressure range of $10^{-4} - 10^{2}$atm. The model is based on the assumption of chemical equilibrium without elemental separation. In this way the equations can be written in a form such that the individual species concentrations are not required explicitly. The thermodynamic coefficients are defined as total properties. Thus, using the model formulation for the total properties, it is possible to write the energy equation in terms of either temperature or total enthalpy. Consequently, the equations can be solved in a similar by schemes that were developed for perfect gas, provided that the curve fits to the total values of the thermodynamic coefficients are available for the ranges of temperatures and pressures of interest. Gupta's model also assumes no ablation or injection of additional gas to the air mixture.

The main motivation for taking this course for solving hypersonic flow problems and not the full thermally and chemically non-equilibrium Navier-Stokes equations is computational efficiency. Solving a reacting Navier-Stokes equations may produce better physical results but with significantly higher cost. The EGM algorithm and its implementation in a compressible Navier-Stokes solver is far from providing complete representation of the flow. However, it is already appears to be very

instrumental in solving complicated configurations in hypersonic flow, as is presented in this work.

The remainder of this paper presents the thermodynamic coefficients computation and model developed by Gupta. Then the thermodynamic coefficient table, a new strategy developed to implement the curve-fit data, is introduced. A number of test cases were identified as potential candidates for the investigation of this approach. The chosen cases were those for which experimental and numerical results are readily available. Each test case is summarized, a brief discussion of the numerical considerations used to simulate the flow is provided, and then evaluates the accuracy of the computed results in terms of heat flux distribution.

II. Computation of thermodynamic coefficients

The current application of the EGM is based on the reports [6–9]. The first report, written by Gupta [6], suggested an accurate curve fits for computing enthalpy, total specific heat at constant pressure, C_p, compressibility factor, Z, molecular viscosity, μ, and total values of thermal conductivity, K, and Prandtl number, Pr, for equilibrium air with temperature range of 500 to 30000K over a pressure range of $10^{-4} - 10^2$atm. The current effort follows this approach.

The implementation of this model in a compressible flow solver is done by collecting all the curve fits presented in [6] into reduced sized tables that contain the total values of C_p, K, μ and Pr as function of pressure and temperature. The temperature is varied between the table's lines while the pressure varies between the table's columns. The entire temperature range of 500 to 30000 K and pressure range of $10^{-4} - 10^2$ atm are broken down to several small intervals, with a minimum temperature interval of 50 K. A logarithmic interpolation relation is applied to obtain values at intermediate pressure and temperature values. For temperature value lower than 600 K the Lemmon [10] fifth order polynomial curve fit is used for C_p approximation . The overlap region between the Lemmon curve fit and Gupta's table is smooth enough in terms of the C_p values obtained with the two models. A pre-processor stand-alone algorithm, which is based on the methodology described above, is used to construct the thermodynamic coefficient tables as function of the local pressure and temperature. This algorithm is utilized by the user in order to generate the thermodynamic coefficient tables prior to running the compressible flow solver.

The underlying assumptions for the ussage of the EGM are listed below. It should be clearly

stated that this model can be applied only for cases where the following assumptions are valid:

1. Equilibrium air calculations - the elemental composition stays constant through the flow field. The masses values are not assumptions.

2. No ablation and injection.

3. Electric field effects are neglected.

4. Chemical equilibrium - all chemical reactions are in balance and the system does not undergo any change in chemical composition.

5. Thermal equilibrium - a single temperature describes the energy modes of all the molecules and it is the same as the temperature of the surrounding.

The nature of the mechanisms through which the gas stores energy, depending on temperature and pressure, is the guidline for the model formulation. As an example, the specific heat at constant pressure C_p is defined as follows [1, 8]:

$$C_p \equiv \left(\frac{\partial h}{\partial T}\right)_p = \sum_{i=1}^{NS} C_i C_{p,i} + \sum_{i=1}^{NS} h_i \left(\frac{\partial C_i}{\partial T}\right)_p \tag{1}$$

where C_i is the mass fraction of species i $(\frac{\rho_i}{\rho})$ obtained from the free-energy minimization calculation method of reference[11], and $\left(\frac{\partial C_i}{\partial T}\right)_p$ is evaluated numerically by differentiating the data from this calculation. The following expression is employed to curve fit the values of C_p, following the form presented by Gupta [6]:

$$C_p = exp(A_{C_p}\chi^4 + B_{C_p}\chi^3 + C_{C_p}\chi^2 + D_{C_p}\chi + E_{C_p}) \tag{2}$$

with $\chi = \ln\left(\frac{T}{10000}\right)$. The polynomial coefficients $A_{C_p}, B_{C_p}, C_{C_p}, D_{C_p} and E_{C_p}$ are given in [6] as function of temperature and pressure values. Once C_p, μ, and K have been computed, it is possible to compute the Prandtl number from its definition, $Pr = \frac{\mu C_p}{K}$. For temperature lower than $500\,K$ and pressure value of 1 atm, the Lemmon [10] polynomial approximation is used for the specific heat at constant pressure, Cp:

$$C_p = exp(A_{C_p}\chi^6 + B_{C_p}\chi^5 + C_{C_p}\chi^4 + D_{C_p}\chi^3 + E_{C_p}\chi^2 + F_{C_p}\chi + G_{C_p}) \tag{3}$$

where $\chi = \ln\left(\frac{T}{10000}\right)$ and the coefficients $A_{C_p} - G_{C_p}$ (different from those present in equation (2)) are defined as follows:

$$A_{C_p} = 0.2518,\ B = 5.49,\ C = 48.18,\ D_{C_p} = 216.70,\ E_{C_p} = 530.02,\ F_{C_p} = 672.82,\ G_{C_p} = 1354.91 \tag{4}$$

The model for the transport properties, thermal conductivity and viscosity coefficients, has a similar form with the appropriate coefficients:

$$\mu = exp(A_\mu + B_\mu\chi + C_\mu\chi^2 + D_\mu\chi^3 + E_\mu\chi^4 + F_\mu\chi^5) \tag{5}$$

where $\chi = \frac{T}{1000}$, and

$$K = exp(A_K\chi^4 + B_K\chi^3 + C_K\chi^2 + D_K\chi + E_K) \tag{6}$$

where $\chi = \ln\left(\frac{T}{10000}\right)$. As for the thermal conductivity and viscosity coefficients, for temperature values lower than $500\,K$ the Sutherland law is applied.

III. Thermodynamic coefficients table

The current study focuses on the computational EGM effectiveness compared to the calorically perfect gas model and the callorically imperfect gas model (Cp=Cp(T)). Three physical models were evaluated:

model 1. Calorically Perfect Gas: The specific heat at constant pressure has a constant value of $1006\,J/KgK$. Both the thermal conductivity and viscous coefficients are computed using the Sutherland law.

model 2. Calorically Imperfect Gas: For the case of a calorically imperfect gas, $Cp = C_p(T)$, has a polynomial representation. Both the thermal conductivity and viscous coefficients are computed by the Sutherland law.

model 3. Equivalent Gas Model: The thermodynamic coefficient, Cp, μ, and K depends on both temperature and pressure as well. This model is more realistic, and permits the analysis of stronger shocks for practical gases. The gas is still considered to be thermally perfect and diatomic.

The EGM model was implemented into a compressible Navier-Stokes solver. Two approaches were considered for the EGM implementation: functional curve fit approach, and thermodynamic coefficient table look-up. The functional curve fit formulation (usually a sine series of order 7) provides a continues definition of the coefficients through all the temperature and pressure range. However, since the application range of temperature and pressure is wide, and the variation of Cp in extreme conditions, i.e. high temperature and low pressure, is dominant, a significant mis-match is produced between the functional fit and the Gupta [6] table. In addition, a multi-term functional formulation is computionaly expensive. This load is significant since the coefficients need to be evaluated at each mesh cell for each iteration or time step. Consequently, significant rise of CPU time and efficiency reduction were observed when this functional fit was applied. This led us to look for a more efficient approach. The second approach consists of a thermodynamic coefficient table look-up, based on the temperature and pressure ranges as defined in Gupta's model. During the iterative process in each cell, the thermodynamic coefficients are evaluated using a logarithmic interpolation process. Since the table's resolution (temperature and pressure intervals), in terms of the tabulated terms, is known upriori and defined during the coefficient table construction phase (prior solving the flow equations), the identification of the relevant "area" in the table, according to a given temperature and pressure, is done by a simple linear transformation. That is to say, no searching procedure is involved, and the property discrete computation is extremely fast. In addition, in order to ensure "smooth" coefficient variables in all the temperature and pressure ranges, the thermodynamic coefficients were linearly averaged (by a moving average algorithm). The dependence of the Cp, μ and K values on the pressure and temperature, is presented in figures (1, 2, 3). The interpolated curve-fit (red line) and Gupta's original values (blue circles) for Cp at a constant pressure of about

10 atm, are presented on the top figure. Also shown for comparison is the Lemmon curve-fit [10] which is defined in temperature range of $300 - 600\,K$. This curve-fit is part of the model in this particular temperature range of $300 - 600\,K$, since its simpler formulation and the relatively smooth variation of the curve-fit properties over the Gupta-Lemmon models The bottom figure shows the variation of Cp with pressure, in a constant temperature of $5000\,K$. The smoothing effect of the averaging process is clearly seen, in particular at the Cp peak region at p=100Pa. Figures (2, 3) shows the variation of the molecular viscosity and thermal conductivity with temperature and pressure, in the same flow conditions.

IV. Total values calculation - pressure, temperature and energy

The local cell-values of total pressure, total temperature and total enthalpy are required for the solution of Navier-Stokes equation. For the case of a calorically perfect gas model the specific heats are constant and the evaluation of the total values of pressure, temperature , enthalpy and energy is straight forward and requires no integration process. For calorically imperfect gas ($C_p = f(T)$) the derivation of the total parameters involves an integration process according to the temperature sub-ranges using pre-defined polynomials. In the case of a real gas calculation the thermodynamic coefficients, Cp, μ, and K depends on temperature and pressure as well. Since the EGM is a table based model (Cp, μ, and K are defined in a discrete manner), the continuous integration process which characterizes the imperfect gas model is replaced by a discrete summation of the thermodynamic coefficients using a given set of temperature and pressure values. The purpose of this chapter is to give a brief description of the total values derivation and to emphasize the different computation approaches between the perfect gas, imperfect gas and EGM. In particular, some of the commonly used assumptions that significantly simplify the total paramaters calculations are not valid any more for real gas. Hence, the more complete and complex integrations of the base formulations are required for that purpose.

The entropy variation is computed from the first and second law of thermodynamics $Tds = dh - \frac{dp}{\rho}$, where s denotes entropy and h is enthalpy. Introducing $dh = C_p(T,p)\,dT$ for a real gas we use the equation of state and obtain the relation

$$\int_T^{T_{tot}} ds = \int_T^{T_{tot}} C_p(T,p)\frac{dT}{T} - R\int_T^{T_{tot}} \frac{dp}{\rho} \tag{7}$$

, where R is the specific gas constant,T is the local temperature and T_{tot} is the total temperature which relates to the maximum enthalpy (total enthalpy, h_{tot}) which the fluid would achieve if brought to rest adiabatically. In an isentropic process ($ds = 0$) the total pressure is evaluated by the following integral

$$P_{tot} = P \cdot \exp\left(\int_T^{T_{tot}} C_p(T,p)\frac{dT}{RT}\right). \tag{8}$$

Once T_{tot} is known, and since the specific heat values are known in each cell, a discrete trapezoidal integration is applied in order to obtain P_{tot} (see further description in the following lines). The first step needs to be the evaluation of the total temperature, T_{tot}.

A. Total temperature computation

For a given value of enthalpy, the total enthalpy, h_{tot}, can be computed by adding the kinetic energy

$$h_{tot} = h + \frac{1}{2}\bar{V}^2. \tag{9}$$

Then, the value of h_{tot} at $T + \triangle T$, at cell i can be estimated from a Taylor series expanded about T (only two terms), that is,

$$h_{tot} = h(T_i + \triangle T) = h(T_i) + \left(\frac{\partial h}{\partial T}\right)_{T=T_i}. \tag{10}$$

Then, evaluation of the right hand side at cell i, for which all quantities are considered as known, is solved iteratively (Euler method) while $\triangle T$ is used in order to construct the next iteration values from the results of the previous iteration. The evaluation process is as follows:

1. Start the iterative process by guessing the local temperature T_i.

2. Use the value T_i to solve $C_p\left(T_i\right)$.

3. Use the value T_i as an integration upper limit of the local enthalpy $h\left(T_i\right) = \int^{T_i} C_p(T)dT$. In practice the integration process is done while the integral boundaries are known, hence the implementation is relatively easy since $C_p(T)$ is a polynomial with constant coefficients.

4. Since $C_p\left(T_i\right)$ and $h\left(T_i\right)$ were estimated from guessed value of T_i, then they will not necesarilly satisy the total enthalpy relation when substituted into the total enthalpy. Hence, by using this equation to construct an improved temperature value T_{i+1} which when added to T_i will bring the local temperature T_i closer to the desired total temperature T_{tot}. That is, the improved temperature is

$$\triangle T = \frac{h_{tot} - h\left(T_i\right)}{C_p\left(T_i\right)}, T_{i+1} = T_i + \triangle T \tag{11}$$

5. At the end of the iterative cycle, the updated temperature is designated T_{i+1}. The iterative process (from step 2 and on) is repeated until the condition $\triangle T \leq \epsilon$ is satisfied. In the current study it was found that the value of $\epsilon = 0.001$ (dimensional value) is a good compromise between accuracy and efficiency. When this is achieved the correct T_{tot} is at hand. Now as T_{tot} is known the complete integration of $\frac{C_p(T)}{RT}$ can be applied.

B. Total values integration

For variable specific heats one must integrate the internal energy and enthalpy by using thier definitions

$$e = \int C_v(T)dT, h = \int C_p(T)dT \tag{12}$$

Since the specific heat values are obtained by an interpolation process using the EGM thermodynamic coefficient tables, the continuous integration process is replaced by a discrete trapezoidal integration over a given temperature range. Hence, the internal energy and enthalpy are computed

by $e = \sum C_v(T) \cdot \triangle T$ and $h = \sum C_p(T) \cdot \triangle T$. For this purpose a constant value of $\triangle T$ is defined by dividing the integration regime into several parallel segments devided by an equal size of $\triangle T$. Since this integration process, for each cell, has to be solved many times during the iterative process toward convergence, it is clear that the size of $\triangle T$ is crucial in terms of computational efficiency. Therefore, the influence of $\triangle T$ on the enthalpy approximation was analyzed as function of the local temperature and pressure values. Results of the relative enthalpy error for different temperature and pressure values, as function of the integration segments number is provided in figure 4. It is clearly seen that for temperature values lower than $500\,K$, $10-50$ segments number range is enough to obtain enthalpy error estimation lower than 1%. For $T > 500K$, with maximum 50 segments, we have reached a satisfactory level of enthalpy error values lower than 0.1%.

V. Test cases configurations

The well known calibration model, HB-2, is the first case that is used to evaluate the EGM. More recently, the Japanese Aerospace Exploration Agency (JAXA) [12] employed HB-2 flare in a series of experiments, which measured force and heat transfer under varying free stream conditions. A sketch of the model is shown in figure (5). The HB-2 model configuration consists of a blunt nose with a curvature radius of 30 mm, a cone with a half vertical angle of 25°, a cylinder with a diameter of 100 mm and a flare skirt with a half vertical angle of 10°. The overall length is 490 mm and the diameter of the base is 160 mm. This model is often used for the calibrations of hypersonic wind tunnels and many reports on measurements are available [12–14]

Another commonly used configuration for hypersonictesting is the blunt cone. The blunt cone is part of test series that were conducted in the California Institute of Technology T5 shock tunnel facility, and it is the second case that is used to evaluate the EGM. This model is a 70° sphere cone, with dimensions given in figure (6). The objectives of this work [15] were to obtain an experimental heat transfer data, and use it to validate the computational tools. All investigations have been carried out under the assumption of steady laminar flow.

The third case is a sharp tip 25°-55° double-cone configuration, as presented in figure (7). This case is one of a test series presented in the thesis dissertation of Tissera [14]. The double-cone model is a suitable test case to evaluate the EGM due to presence of complicated flow features such as interaction between a shock wave and a separated flow. The research facilities at Caltech, Calspan (CUBRC), and Princeton university were used to produce a large experimental data base for this test case [16, 17]. The Reynolds and Mach number were chosen in such a way to ensure that the flow over the double-cone remains laminar.

VI. Computational model

A. Numerical set-up

The flow field computations were performed using a compressible Navier-Stokes solver. This code has been used extensively for subsonic, transonic, supersonic and hypersonic flow configurations. It is a parallel multiblock finite volume code that solves the 3D full Navier-Stokes equations for gas in chemical and thermal equilibrium. The discretization of the governing equation is done by finite volume approach with a central formulation over structured meshes. The convective terms are computed by Roe flux splitting upwind scheme with Van-Albeda limiter. Viscous fluxes are computed to second order accuracy using a central difference approach. The residual smoothing is made by employing an explicit 5th order multistage Runge-Kutta algorithm. The thermodynamic coefficients, specific heat at constant pressure, thermal conductivity and viscosity coefficient are evaluated by polynomial curve-fits of temperature and pressure by using the table model presented by Gupta [6]. For this purpose a stand alone pre-processor has been developed for constructing thermodynamic coefficient table file according to the flow conditions (pressure and temperature) we are solving. These tables serve as an input to the compressible flow solver. The computational coordinate system is x, y, and z axes, while x is in the stream-wise direction, y vertical, and z span-wise. The origin is located at the stagnation points.

B. Boundary conditions

Due to the short test duration time (i.e., in HIEST a typical experiment takes about 10 msec), the model temperature does not vary significantly during the shot, therefore an isothermal wall is assumed, with a constant temperature of 300 K for all cases. Free stream conditions are enforced at the far-field boundaries. Table (1) collects the numerical flow conditions with two stagnation enthalpy values for each test case. The stagnation and free stream conditions for the following simulations were obtained from the JAXA tests published in 2006 [12] (for the HB-2 model), NASA Aims shock tunnel [15] (blunt cone model), and [14] for the double cone model.

C. Computational mesh

Both the HB-2, blunt-cone and double-cone configurations do not give rise to complicated flow features. However, in order to properly capture the heat transfer over the surface, it is extremely important to use a sufficiently refined computational mesh. The accuracy of the heat transfer predicted near the wall is strongly dependent on the quality of the grid and the clustering near the wall. For this purpose several levels of grid refinement have been checked to assess the effect on the numerical accuracy, while the total number of grid cells ranges from 200,000 to 1,000,000 cells. The minimum cell's height on the wall h_{min} was changed from 100 μm to 1 μm. A typical grid clustered towards the wall is presented in figures (8-10) for the HB-2, blunt cone and double cone models. Total enthalpy values of $H0 = 4MJ/Kg$, $H0 = 8MJ/Kg$, and $H0 = 10MJ/Kg$ were employed for mesh independence test for the cases of HB-2, blunt cone and double-cone models, respectively. The effects of the grid refinement on the quality of the numerical solution are described in figures (8-10) for the three models, and for three grid levels. The heat transfer distribution along the body is normalized by the stagnation point value (peak heating). It is clearly seen that the numerical solution of the flow fields is highly sensitive to the grid refinement, and the prediction of the locally normal shock, and the correct shock layer are the most critical aspects of the present simulations. The difference in the heat transfer values obtained in the three grid levels for both models is significant while moving from $h_{min} = 100\mu m$ to $h_{min} = 10\mu m$. The difference between

$h_{min} = 10\mu m$ and $h_{min} = 1\mu m$ is minor and grid resolution studies confirmed that the computed heat transfer values are grid converged. The total number of cells for the final grids is 500,000, 200,000 and 10^6 cells for the HB-2, blunt-cone and double-cone models, respectively.

VII. Results

The present investigation employed three test cases, namely HB-2, blunt-cone and double-cone models. The three models were tested under caloricaly perfect gas conditions, caloricaly imperfect gas conditions and EGM, with the same flow conditions (total pressure, total enthalpy and Mach number) according to the specific test case involved. The experiments were conducted using shock tube wind tunnel. The shock tube tunnel flow that reaches the test section is usually thermally and chemically non-equilibrium because of the extreme high pressures and temperatures in the test section. This fact limited the quality of comparison with the EGM computation. The comparison of the results of the different models is listed below.

A. HB-2

Figures (VII A, VII A) presents the shock layer, obtained by the three models under discussion, at total enthalpy of $H0 = 4MJ/Kg$ and $H0 = 7.8MJ/Kg$ respecively. One can observe the typical features for this type of flow, which are the strong detached shock wave in front of the model, and the expansion wave formed on the shoulder behind the nose. The provided temperature contours reveal the major influence of the EGM model: First, lower rise of temperature in the stagnation region, compared with the results of the two other models. Second, the solution utilizing the EGM predicts a thinner shock layer (especially in the stagnation region) than the results of the two other models. As the Mach number increases, more of the translational energy goes into excitation of the internal energy modes of the gas, which means less energy is available for translation downstream [2]. Consequently, the temperature rise across the shock, obtained by the ideal gas

model, is higher than that obtained by the two other models, which account for internal energy transfer. This means that the temperature rise across the shock is less for a calorically imperfect gas than for an ideal gas. The pressure rise accross the shock wave near the stagnation point ($x1 = -0.005, y1 = 0.004, z1 = 0.0, x2 = -0.002, y2 = 0.004, z2 = 0.0$) is nearly constant in all the three models, while only 4The reduced temperature rise causes an increase in the density rise across the shock. In case of a hypersonic vehicle bow shock, we see that this increase in density is offset by a decrease in flow area to conserve mass, and this is the mechanism by which the shock moves closer to the body, as it is clearly seen in the EGM case. The shock layer maximum temperature obtained with the EGM is nearly 15% lower than obtained in the calorically perfect gas model. For example, in the case of $H0 = 4MJ/Kg$ the maximum static temperature obtained is 3690K for the EGM compared to 3150K obtained in the calorically perfect gas model.

The computed heat transfer distribution along the HB-2 configuration is presented in figures (VII A, VII A), for the calorically perfect gas, calorically imperfect gas, and EGM. The computed results are also compared with experiment measurments [12]. The comparison between computed results and experimental data shows a good agreement for heat flux in high enthalpy ($7.8MJ/Kg$) and low enthalpy($4MJ/Kg$) cases, especially in the stagnation point area. In contrast the separation zone, has not been correctly captured even in the EGM. At this time, reason for this discrepancy is unknown. Since a real gas is involved, the test section conditions were derived by using an empirical correlations for calorically and imperfect gases. Therefore, it can be speculated that the experimental free stream conditions (Mach number, total pressure and total temperature) listed may contain inaccuracies and need to be clarified.

B. Blunt-cone

The static temperature contours over the blunt-cone configuration symmetry plane are presented in figures (VII B) at zero angle of attack and stagnation enthalpy of $H0 = 11.4MJ/Kg$. In figure (VII B) the same properties are presented for high stagnation enthalpy of $H0 = 19.3MJ/Kg$ and 8° angle of attack. Laminar Navier-Stokes were employed for the solution of the low enthalpy case. However, the high level of heat flux which was reported in the experiment [15] clearly indicated on turbulent flow. That way turbulent formulation with Spalart Allmaras turbulence model were used for this case. In both cases one can see that the temperature is suddenly increased across the shock and continues to rise until approaching the isothermic wall. Similar to HB-2 model, the EGM prediction of the shock layer is thiner than that obtained by the other models. The shock layer maximum temperature obtained with the EGM is nearly 50% lower than the one obtained with the calorically perfect gas model, for $H0 = 11.4MJ/Kg$. For $H0 = 19.3MJ/Kg$ the resultant maximum temperature was 60% lower than obtained by the calorically perfect gas model.

Figures (VII B, VII B) shows a comparison of the predicted and measured heat transfer rates for the blunt-cone configuration, for the two enthalpy cases $H0 = 11.4MJ/Kg$ and $H0 = 19.3MJ/Kg$, respectively. The experimental results were taken from [15]. In both cases, it is evident that the calorically perfect gas model significantly over predicts the heat flux, compared with experiments [15], while the EGM properly reproduced the measurements, especially near the stagnation point that is located at $y = 0$. Still, the EGM results are much higher than the experimental results at $y > 0.06m$, near the shoulders. In the high enthalpy case, $H0 = 19.3MJ/Kg$, similar to the $\alpha = 0^\circ$ results, the calorically perfect gas solutions obtained are more then 1.5 times larger than the experimental heating levels at $y = 0$. In the case of $H0 = 19.3MJ/Kg$ the heat flux distribution is not symmetric around the stagnation point since an angle of attack of 8 deg is involved. As for the EGM results, there is a good agreement at $y = 0$ but as we go further towards the cone shoulders the agreement deteriorates. The stagnation point for this case is located at approximately $y = -0.07m$.

The computed heat transfer shows an unphysical of a local minima in the stagnation region. The high pressure and heat transfer clearly effects the nose tip temperature and heat flux values. This behavior is often called "carbuncle" phenomenon, which can be partially solved by optimizing the grid around the nose. It is possible that a more accurate relaxation method (than the fifth order Runge-Kutta) in the boundary layer could result in a better convergence conditions. At present, no attempt has been made to account for this effect in the EGM. EGM,to be accounted for in future implementations.

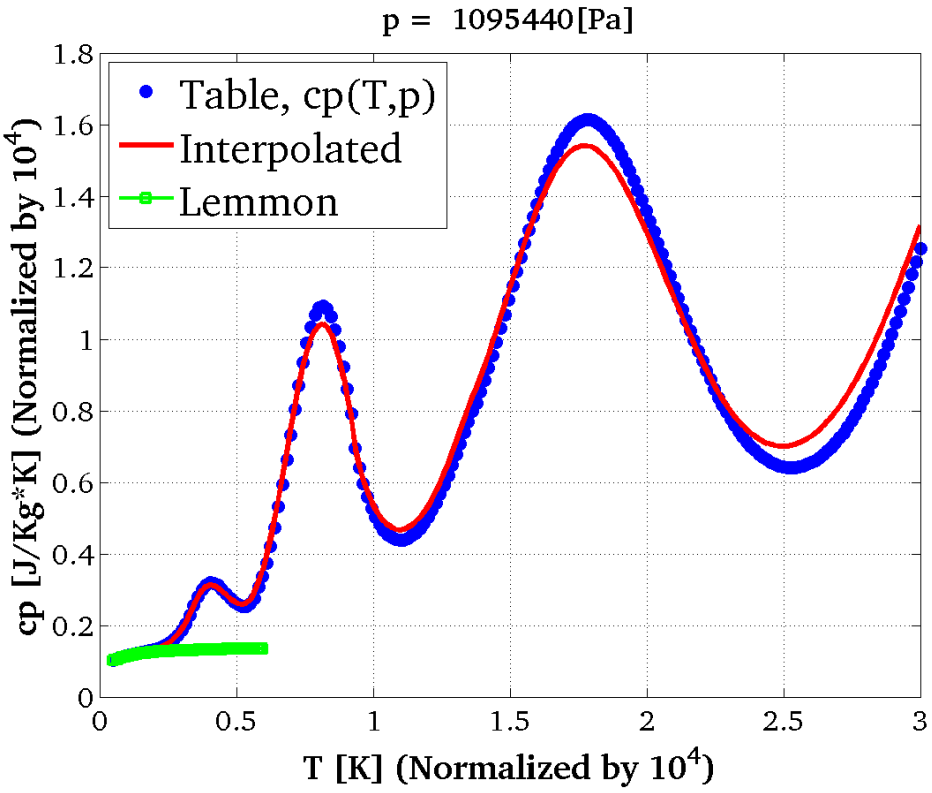

(a)

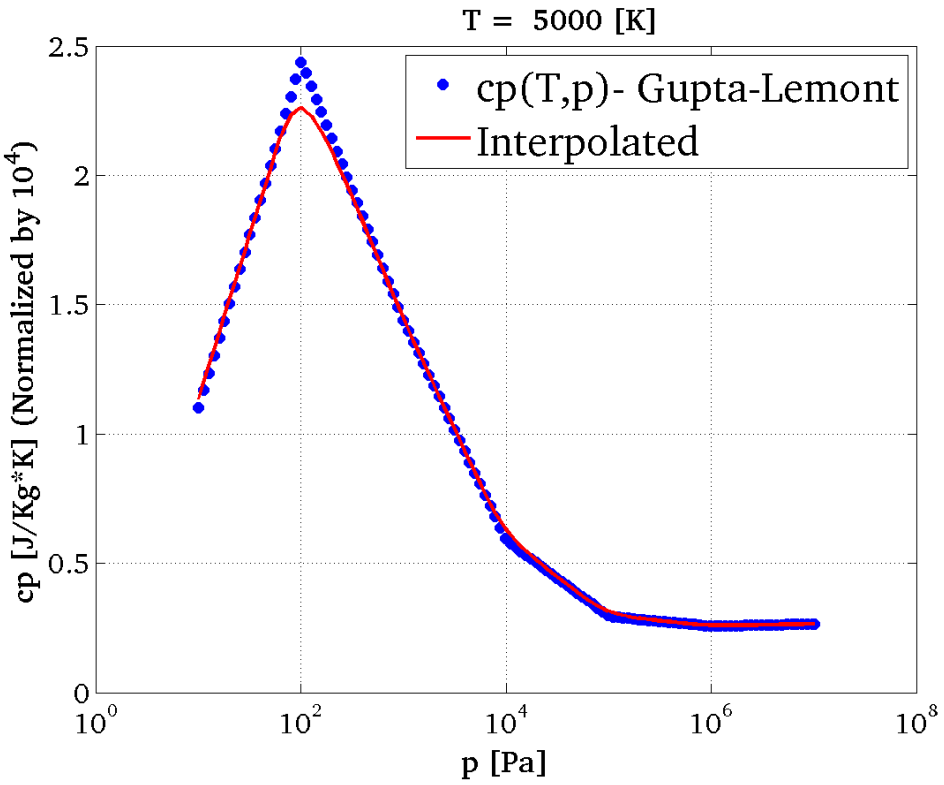

(b)

Fig. 1 (a) Cp, as function of temperature, at constant pressure of 10 atm. (b) Cp, as function of pressure, at constant temperature of $5000K$

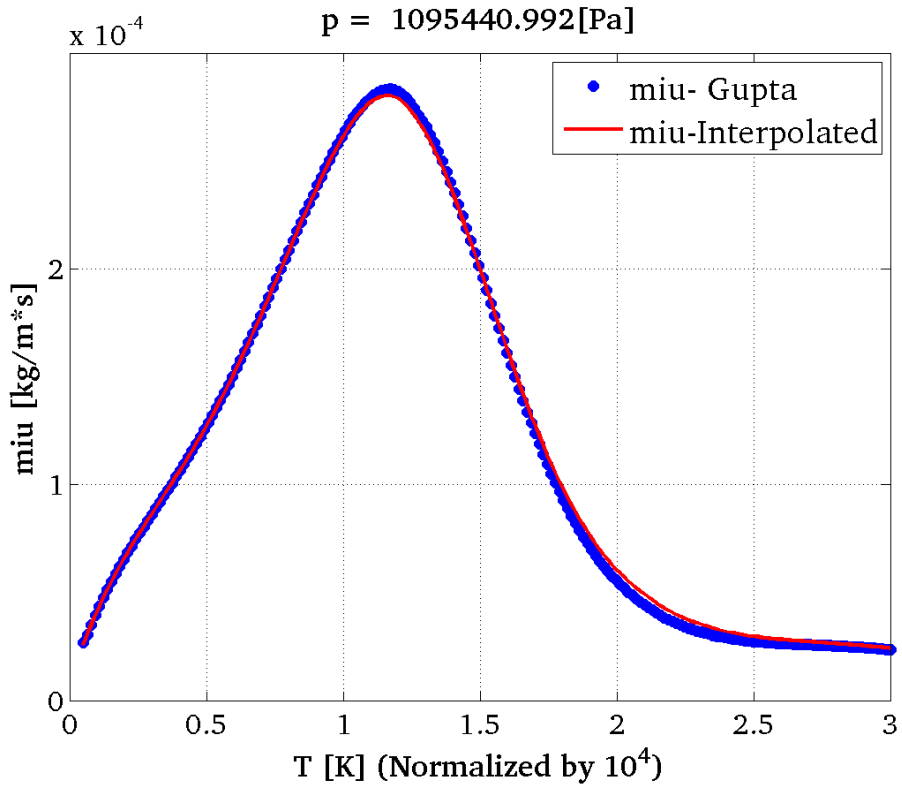

(a)

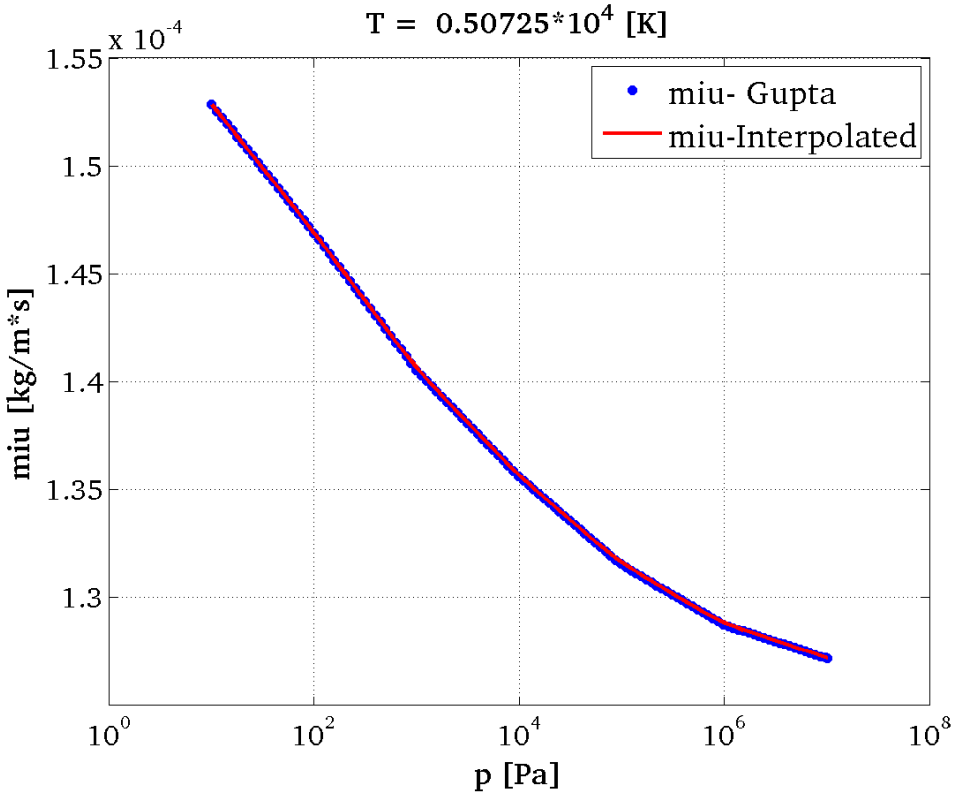

(b)

Fig. 2 (a) μ, as a function of temperature, at constant pressure of 10 atm. (b) μ, as a function of pressure, at constant temperature of $5000 K$.

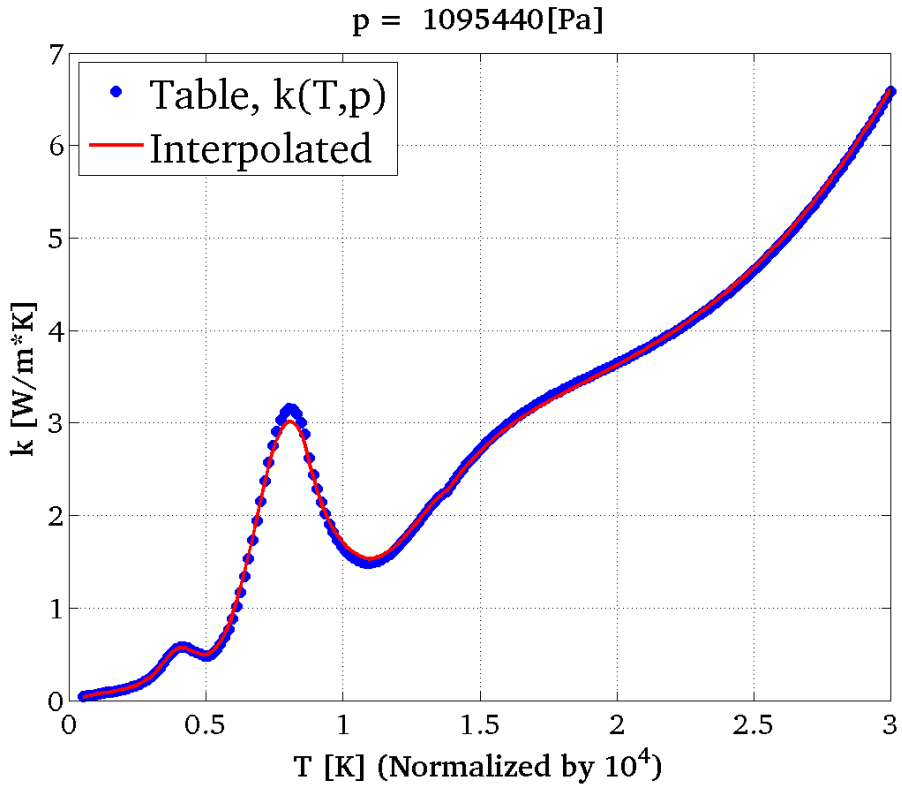

(a)

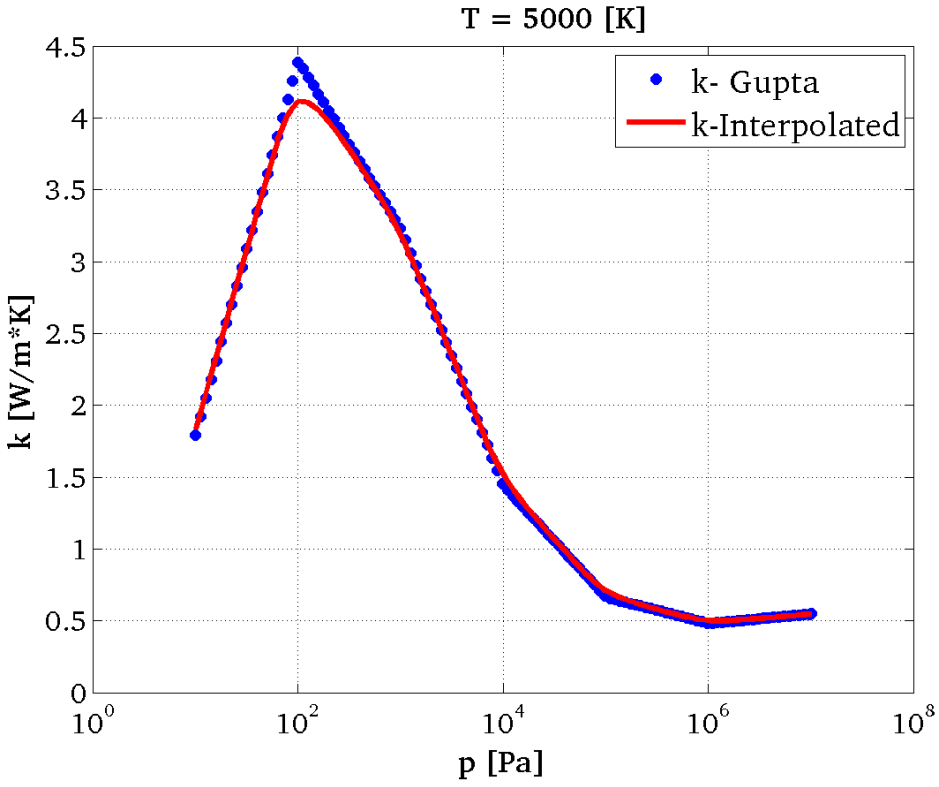

(b)

Fig. 3 (a) K as a function of temperature, at constant pressure of 10 atm. (b) K as a function of pressure at constant temperature of 5000 K.

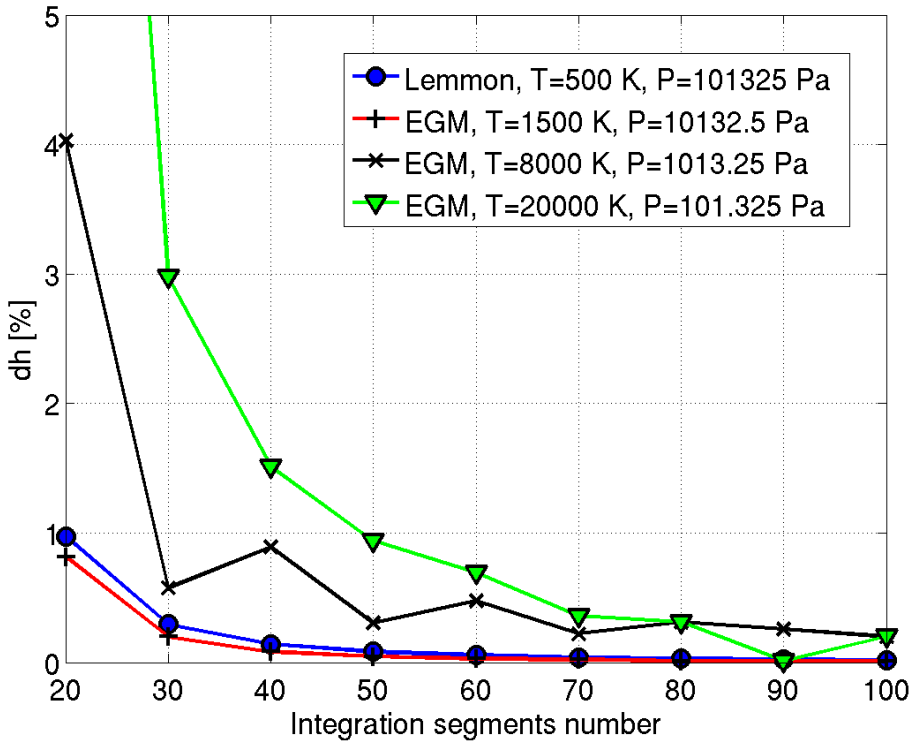

Fig. 4 Enthalpy error in % Vs. different integration segments number.

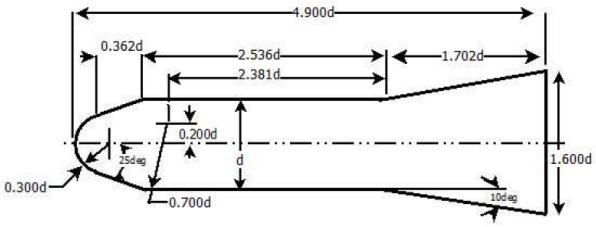

Fig. 5 The HB-2 model scheme.

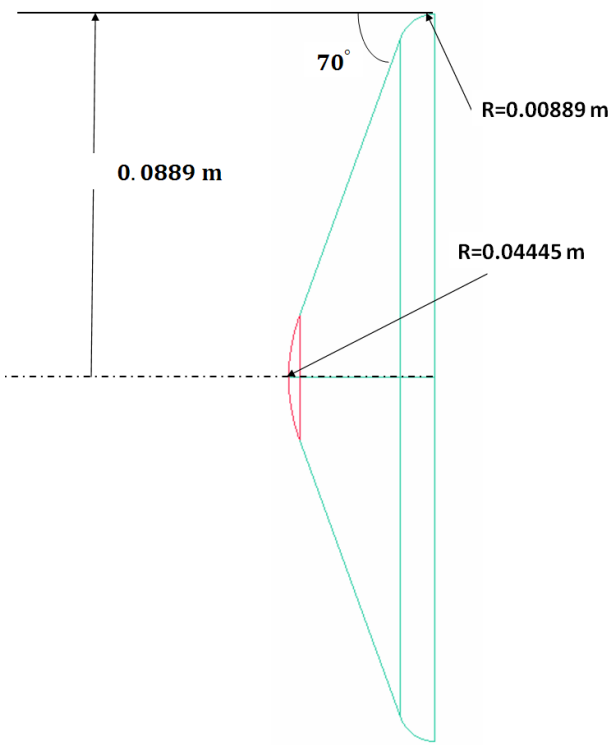

Fig. 6 The blunt-cone model scheme.

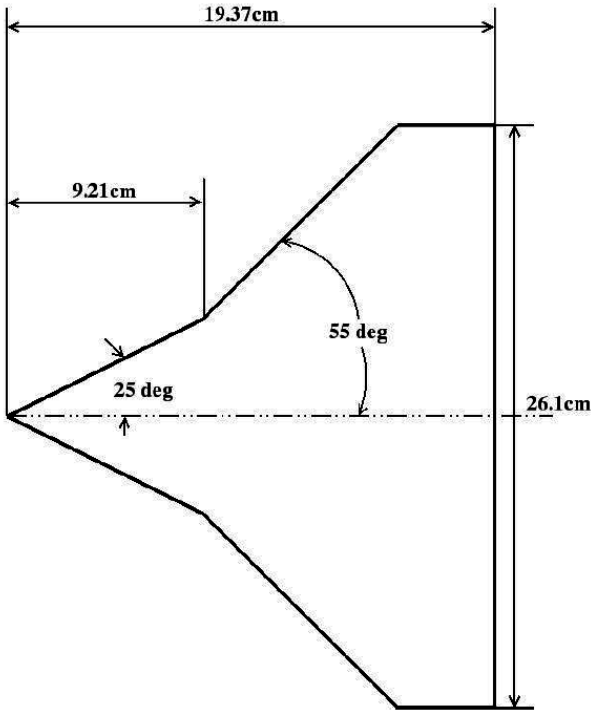

Fig. 7 The $25^\circ - 55^\circ$ sharp-tipped double-cone model scheme.

Table 1 Free-stream and stagnation conditions.

Case	Configuration	Stagnation		Free stream			
		Enthalpy	Pressure	Temperature	Mach	AoA	Reynolds
		[MJ/Kg]	[MPa]	[K]	[-]	[deg]	[-]
1.	HB-2	4.0	0.002	300	7.5	0	336,211
2.	HB-2	7.8	0.00564	709	6.67	0	294,000
3.	Blunt-cone	11.4	20.8	1287	6.03	0	577,612
4.	Blunt-cone	19.3	50.5	2670	5.2	8	1,302,473
5.	Double-cone	10.0	6.67	576	8.87	0	80,614
6.	Double-cone	10.0	12.4	268	11.52	0	85,286

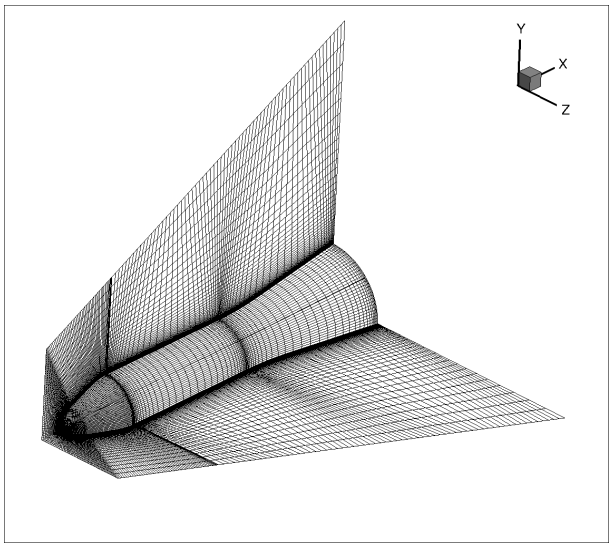

(a)

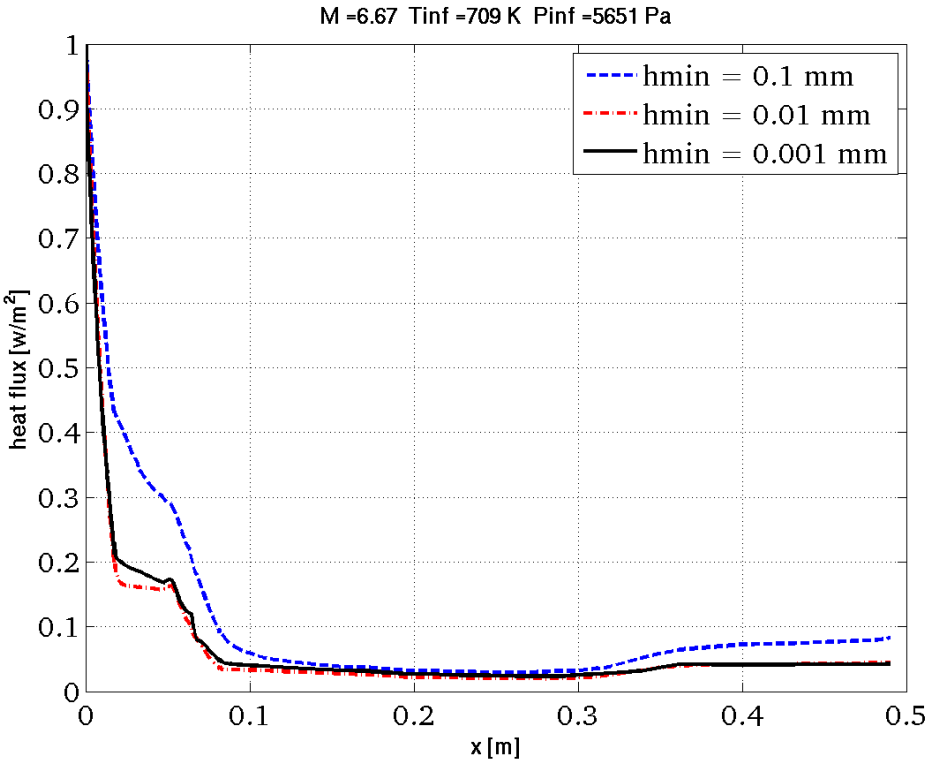

(b)

Fig. 8 (a) The HB-2 Quarter model structured grid. (b) Grid dependence study of the normalized heat flux at $H_0 = 4MJ/Kg$

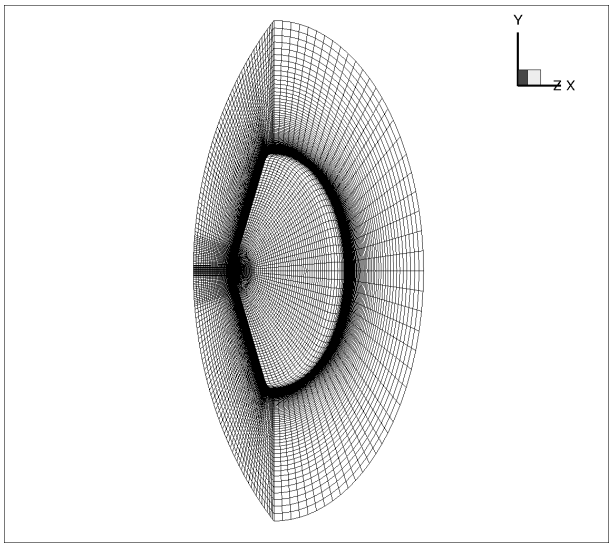

(a)

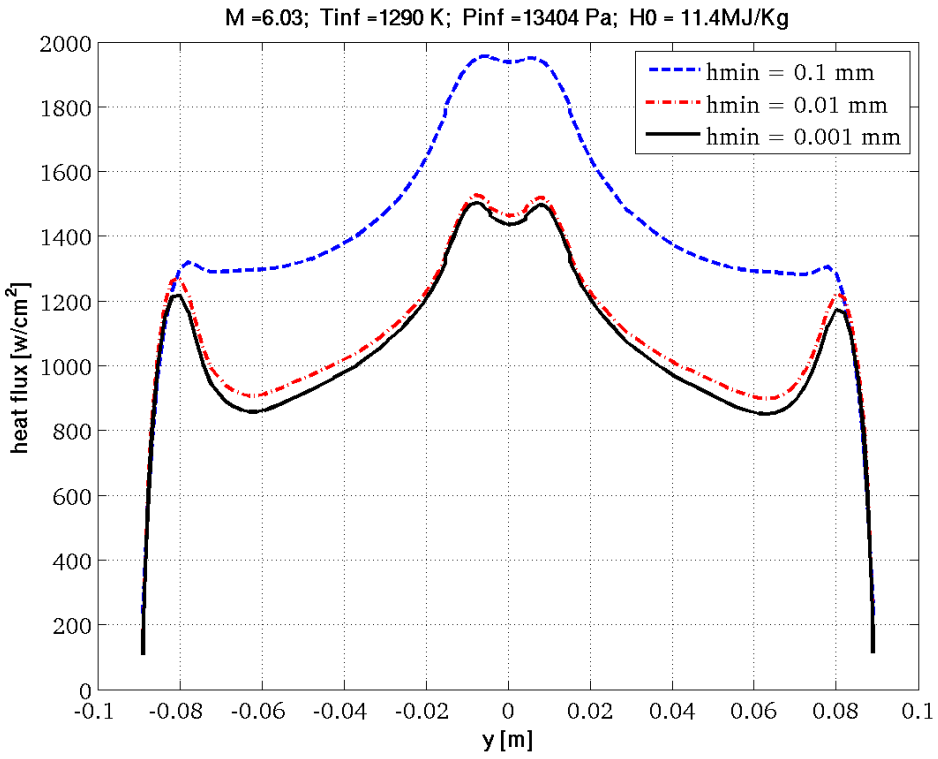

(b)

Fig. 9 (a) The blunt-cone grid topology. (b) Grid dependence study on the normalized heat flux at $H_0 = 11.4MJ/Kg$.

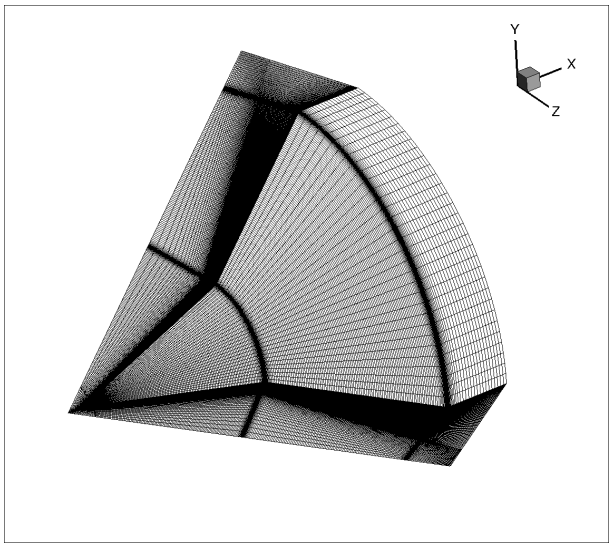

(a)

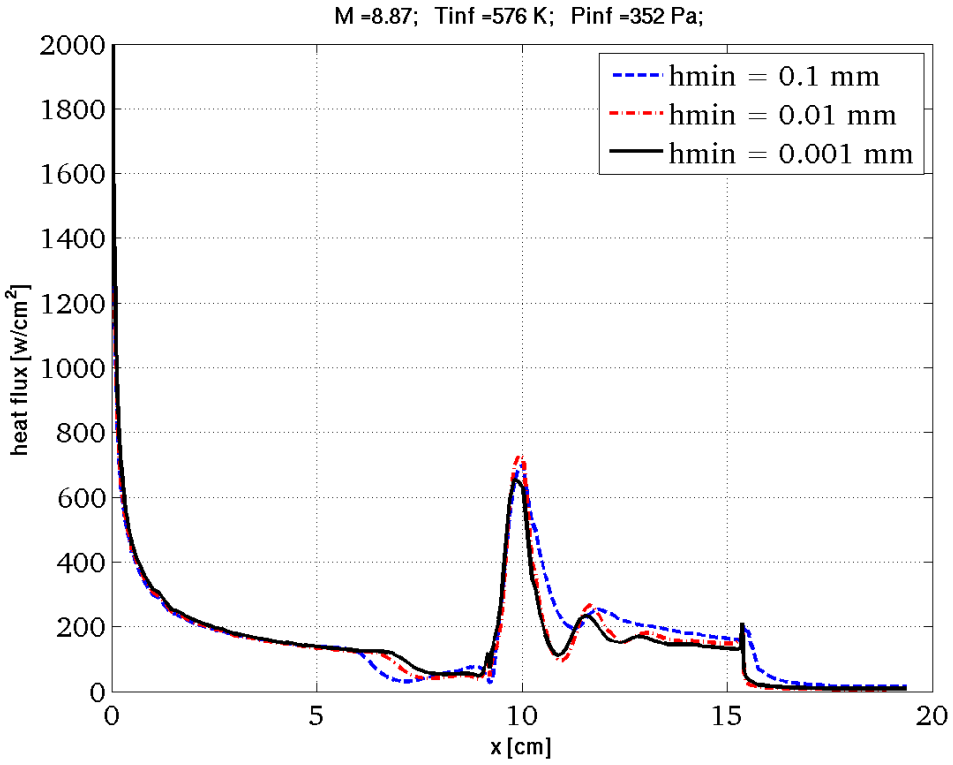

Fig. 10 (a) Computational mesh of the double-cone model. (b) Grid dependence study of the heat flux distributions at $H_0 = 10MJ/Kg$.

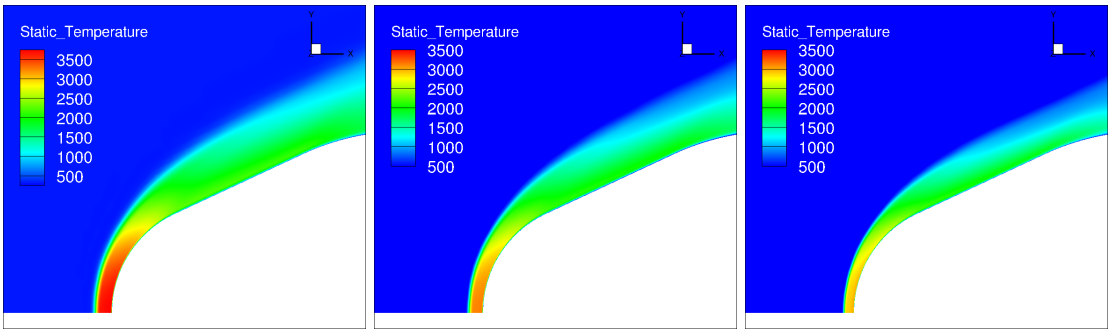

(a) (b) (c)

Fig. 11 Static temperature contours of the HB-2 model for calorically perfect gas (a), callor-icaly imperfect gas (b) and EGM, (c), for $H_0 = 4MJ/Kg$, $M_\infty = 7.5$.

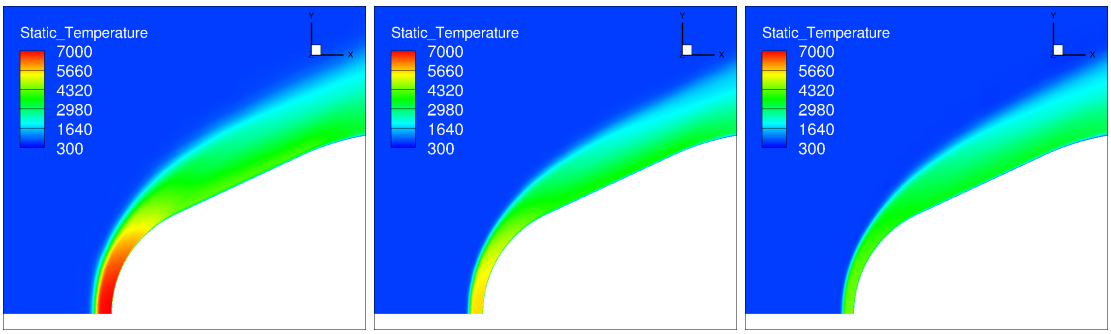

(a) (b) (c)

Fig. 12 Static temperature contours of the HB-2 model for calorically perfect gas (a), callor-icaly imperfect gas (b), and EGM (c), for $H_0 = 7.8MJ/Kg$, $M = 6.67$.

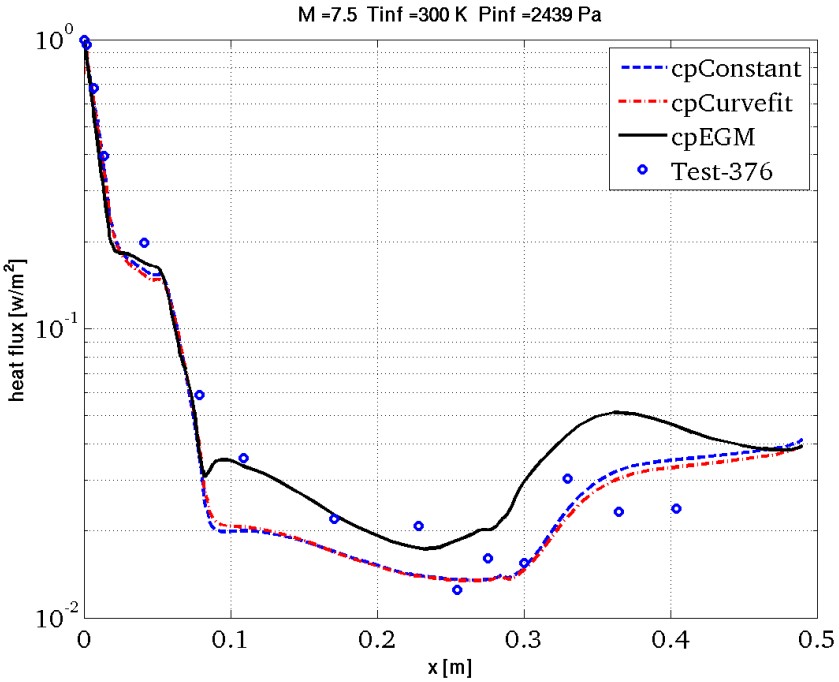

Fig. 13 The HB-2 computed heat flux for calorically perfect gas (blue), calloricaly imperfect gas (red), and EGM (black), for $H_0 = 4MJ/Kg$, $M_\infty = 7.5$.

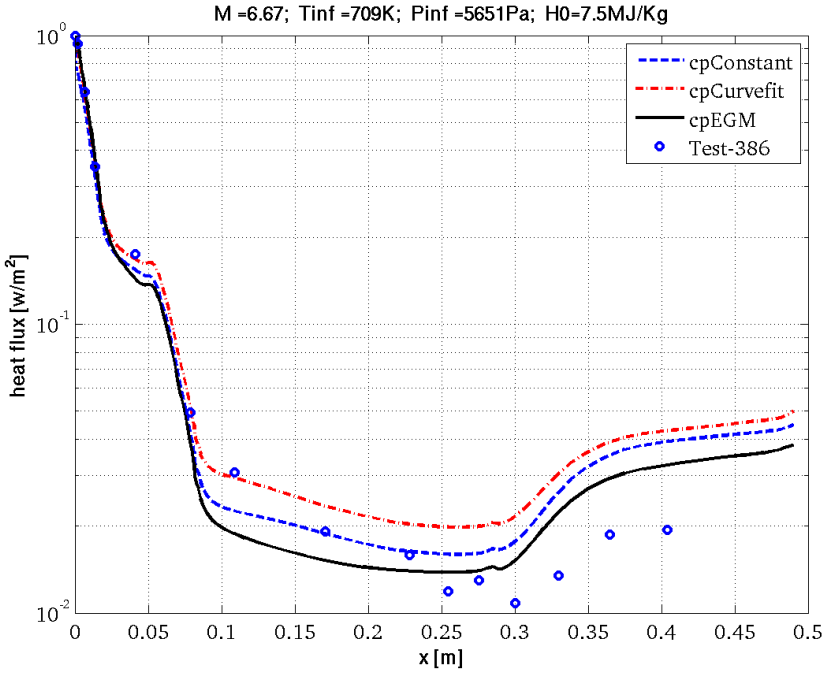

Fig. 14 The HB-2 computed heat flux for calorically perfect gas (blue), calloricaly imperfect gas (red), and EGM (black), for $H_0 = 7.8MJ/Kg$, $M_\infty = 6.67$.

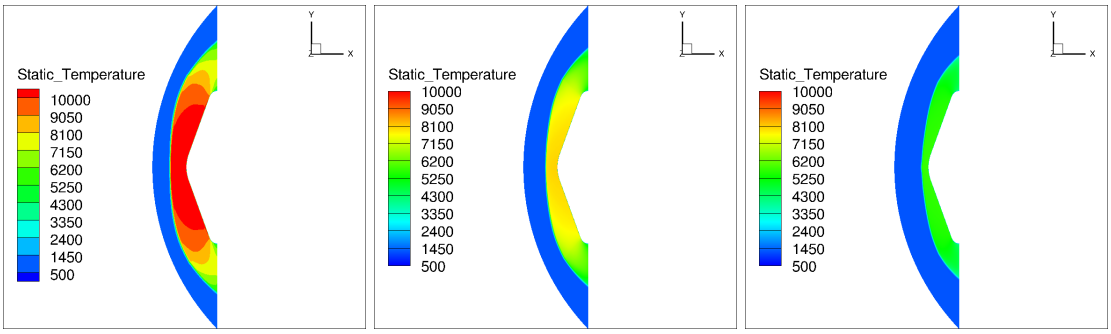

(a) (b) (c)

Fig. 15 Static temperature contours of the cone model for calorically perfect gas (a), calloricaly imperfect gas (b), and EGM (c), for $H_0 = 11.4MJ/Kg$, $M = 6.03$.

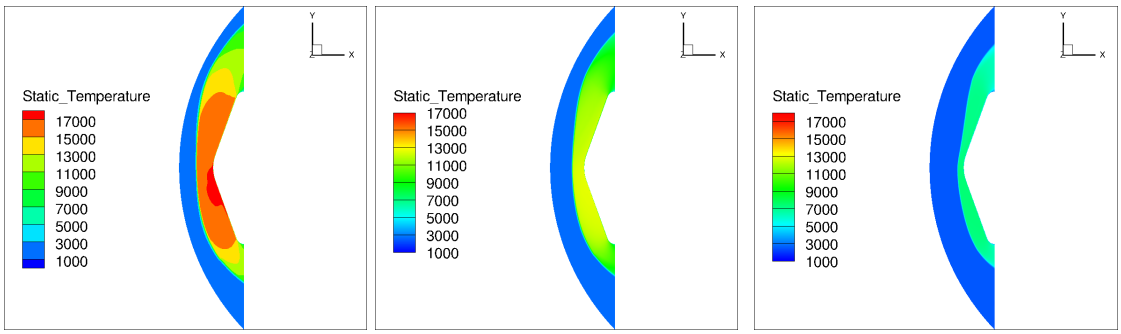

(a) (b) (c)

Fig. 16 Static temperature contours of the cone model for calorically perfect gas (a), calloricaly imperfect gas (b), and EGM (c), for $H_0 = 19.3MJ/Kg$, $M = 5.2$.

C. Double-cone

Two test runs for the double cone configuration have been conducted for the purpose of validation. The flow conditions were taken according to runs 42 and 43 presented in [14]. Both cases have high enthalpy conditions (approximately $10\,MJ/Kg$) and are simulated using caloricaly perfect gas, calorically imperfect gas, and EGM. The heat transfer distributions from the numerical simulations are compared with the experimental and computed data presented in [14]. The flow features that develop around the double-cone model are complicated than those obtained with both the HB-2 and the blunt-cone configurations. The flow structure typical of the double-cone is presented in the visualization of the temperature contours in figures (VII C) (cases 5 and 6), identifying the shock positions, the details of the separation region and the under expanded jet along the second cone. The first cone generates an incident shock which is close to the cone's surface. The incident shock interacts with the second shock generated by the second cone. The shocks interactions causes a pressure rise and flow separation. Again, the EGM prediction for the temperature rise in the shock layer is smaller than that obtained by the two other models. Furthermore, the shock location that is identified by the EGM model is closer to the solid surface that obtained by the other models.

Figures (VII C-VII C) shows a comparison of the predicted and measured heat transfer rates and pressure values for cases 5 and 6. The separation point is indicated in the experiment by a rapid decrease in heat transfer, and similarly the reattachment point is identified by a rapid increase in heat transfer. It appears that the separation point has not been correctly captured by the numerical simulation, and the maximum heat transfer simulated value is located about 7-8 mm upstream compared to the location identified in the experiment [14]. Concerning the EGM and experimental results, both Cp and q values are well compared. The seperated flow characterized by a nearly constant heat transfer and pressure values.

VIII. Conclusions

Self consistent models have been used for total specific heat at constant pressure, thermal conductivity, and viscosity coefficients of equilibrium air from $500\,K$ to $30000\,K$ and pressure range of $10^{-4} - 100$ atm. The derivation presented here of the EGM is based on the 11-species air model published by Gupta [6]. Practically, the thermodynamic coefficients were computed and arranged in form of a table model while a logarithmic interpolation relation is provided to obtain values at a given temperature and pressure. Further, a linear averaging procedure is performed for the thermodynamic coefficients in order to ensure smooth and continuous values through all the temperature and pressure ranges. The EGM was implemented in a compressible Navier-Stokes solver and a code validation study for high-enthalpy real-gas flows has been employed. Three test cases were compared with data at enthalpy levels of up to $19\,MJ/Kg$ in an ambient air.

EGM model was formulated and implemented in order to facilitate simulation of hypersonic flow without the complexity of full thermally and chemically non-equilibrium model. Solving a reacting Navier-Stokes equations may produce better physical results but with significantly higher cost. The EGM algorithm and its implementation in a compressible Navier-Stokes solver is far from being optimal. However, it already appears to be very instrumental in solving complicated configurations in hypersonic flow, as is presented in this work. Although the EGM offers realistic predictions, more development is needed to achieve better quantitative agreement with measurements.

The main observations from the test cases investigation are as follows:

- It was observed that the HB-2 computations, performed for stagnation enthalpy values of $4\,MJ/Kg$ and $7.8\,MJ/Kg$, well predicted the heat flux over the nose region but under predicted the heat flux over the main body (especially in $M_\infty = 6.67$). A possible explanation for this discrepancy can be the uncertainty in the free-stream conditions.

- In the blunt-cone model simulation the laminar EGM predictions well matched the experimental data, mainly near the stagnation region. However, the heating rate at the cone's shoulders was over-predicted.

- In the double-cone model the agreement between the EGM computations and experiment values is reasonable for the surface pressure, but there is a discrepancy in the predicted heat transfer rates for the three physical models (calorically perfect gas, imperfect gas, and EGM). The computations agree best for the EGM in Run 43 ($M_\infty = 11.5$). The heat transfer rate is remarkably good, with all of the flow features captured.

IX. Acknowledgments

I would like to thank Dr. M. Shuser and Mr. M. Kidar for their support in the first stage of this research work. Their help and advice are greatly appreciated.

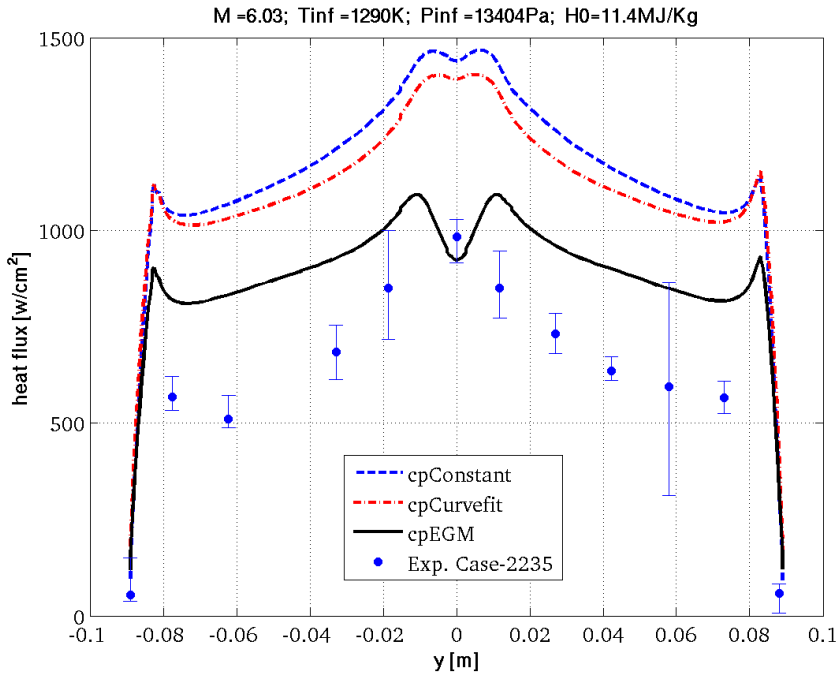

Fig. 17 Laminar heat flux of the blunt cone model for perfect gas (blue), imperfect gas (red), and EGM (black). The simulation conditions are: $H_0 = 11.4MJ/Kg$, $M = 6.03$.

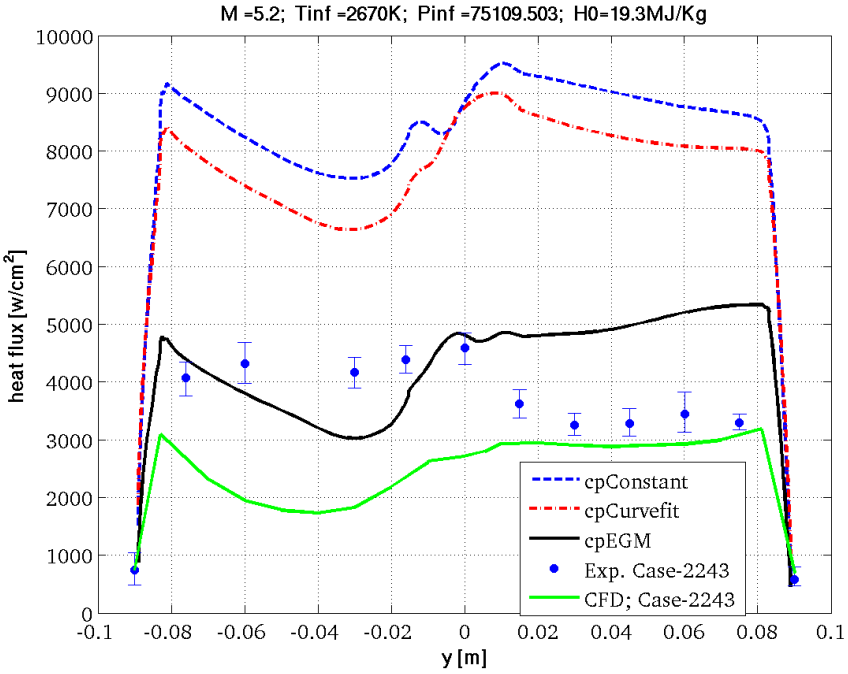

Fig. 18 Turbulent heat flux of the blunt-cone model for perfect gas (blue), imperfect gas (red), and EGM (black), for $H_0 = 19.3MJ/Kg$, $M_\infty = 5.2$.

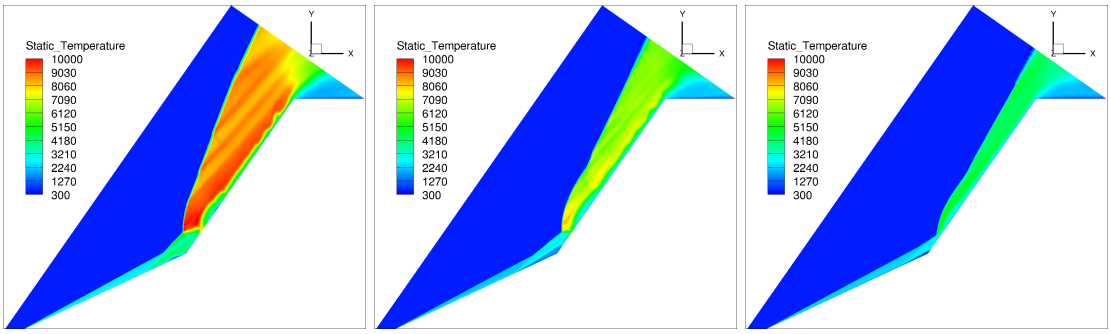

(a) (b) (c)

Fig. 19 Static temperature contours of the double-cone model for perfect gas (a), imperfect gas (b), and EGM (c), for $H_0 = 10MJ/Kg$, $M_\infty = 8.87$.

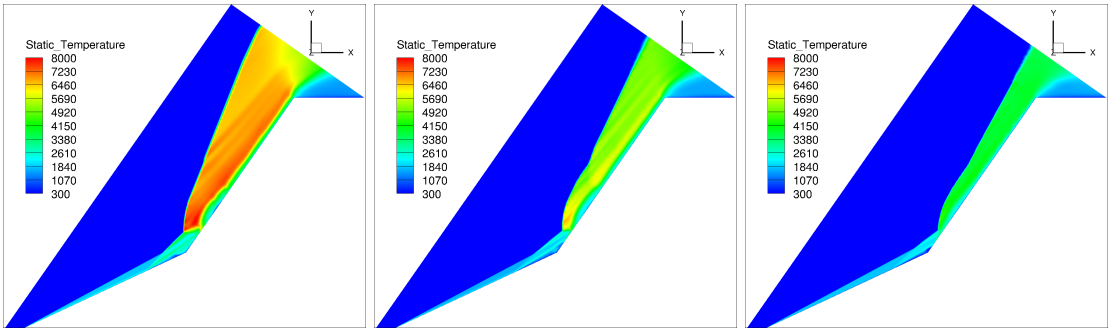

(a) (b) (c)

Fig. 20 Static temperature contours of the double-cone model for perfect gas (a), imperfect gas (b), and EGM (c), for $H_0 = 10MJ/Kg$, $M_\infty = 11.5$.

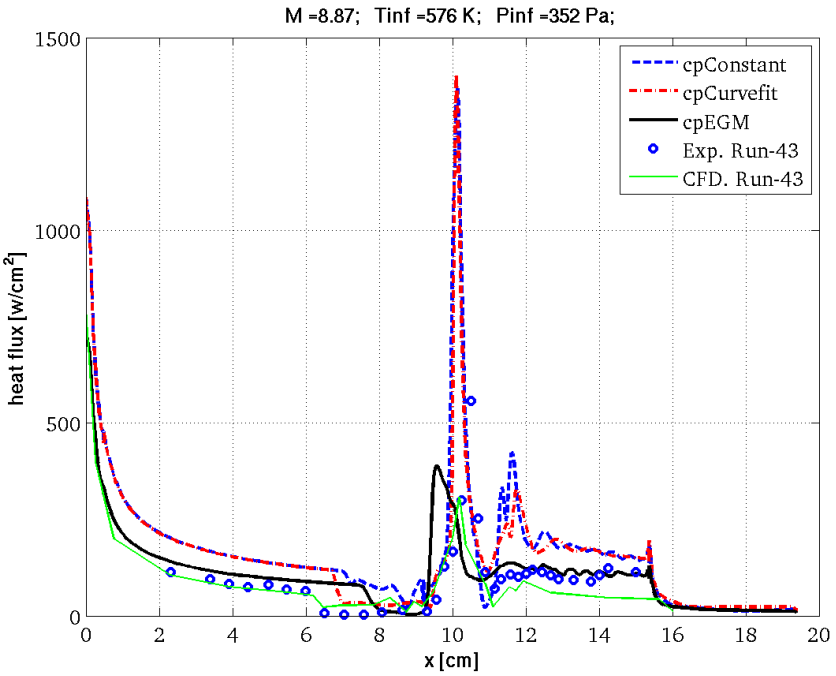

Fig. 21 Heat flux of the double-cone model for perfect gas (blue), imperfect gas (red), and EGM (black), for $H_0 = 10MJ/Kg$, $M_\infty = 8.87$.

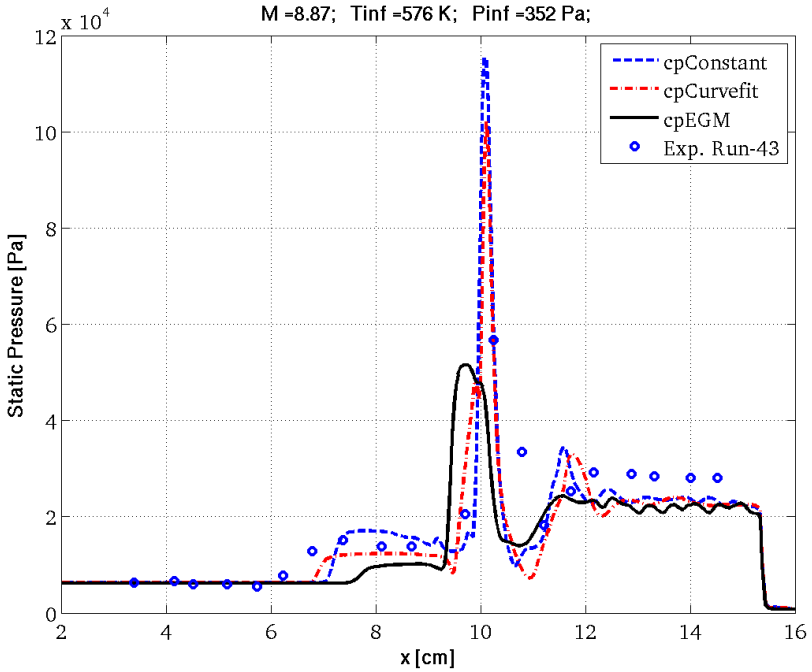

Fig. 22 Static pressure of the double-cone model for perfect gas (blue), imperfect gas (red), and EGM (black), $H_0 = 10MJ/Kg$, $M_\infty = 8.87$.

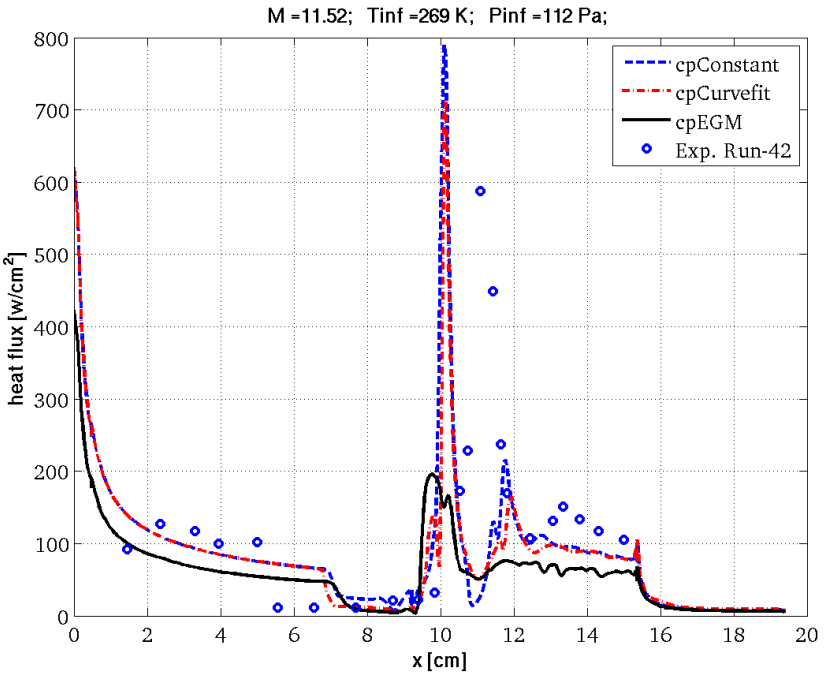

Fig. 23 Heat flux of the double-cone model for perfect gas (blue), imperfect gas (red), and EGM (black), for $H_0 = 10MJ/Kg$, $M_\infty = 11.5$.

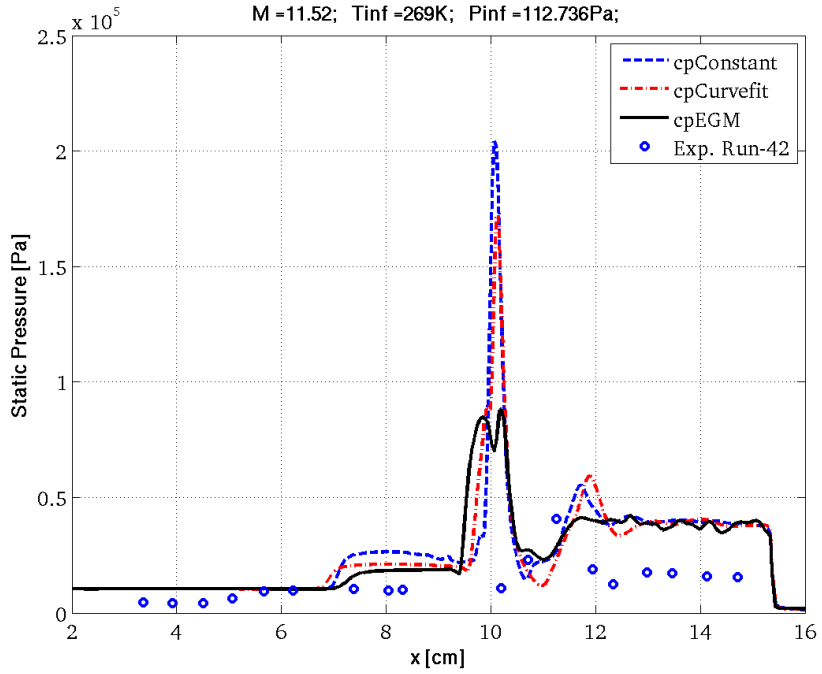

Fig. 24 Static pressure of the double-cone model for perfect gas (blue), imperfect gas (red), and EGM (black), for $H_0 = 10MJ/Kg$, $M_\infty = 11.5$.

[1] Anderson, J. D., *Hypersonic and High Temperature Gas Dynamics*, McGraw-Hill, 1989.

[2] Fletcher, D. G., "Fundamentals of Hypersonic Flow-Aerothermodynamics," Tech. rep., von Karman Institute, Belgium, 2004.

[3] Candler, G. V., *The Computational of Weakly Ionized Flow in Nonequilibrium*, Ph.D. thesis, Stanford University, 1988.

[4] P. A. Gnoffo, R. N. G. and Shin, J. L., "Conservation Equations and Physical Models for Hypersonic Air Flows in Thermal and Chemical Nonequilibrium," Tech. Rep. 2867, NASA, Langley, Hampton, Virginia, 1989.

[5] Lee, J. H., "Basic Governing Equations for the Flight Regimes of Aeroassisted Orbital Tranfer Vehicles," *Thermal Design of Aeroassisted Orbital Transfer (AIAA)*, Vol. 96, 1985, pp. 3–53.

[6] Roop N. Gupta, Kam-Pui Lee, R. A. T. J. M. Y., "Calculations and Curve Fits of Thermodynamic and Transport Properties of Equilibrium Air to 30000K," Tech. Rep. 1260, NASA, 1991.

[7] Yos Jerrold M., Thompson Richard A., L. K.-P. G. R. N., "A Review of Reaction Rates and Thermodynamic and Transport Properties for an 11-Species Air Model for Chemical and Thermal Nonequilibrium Calculations to 30000K," Tech. Rep. RP-1232, NASA, 1990.

[8] Frederick, H. C., "Approximations for the Thermodynamic and Transport Properties of High-Temperature Air," Tech. Rep. TR-R-50, NASA, 1959.

[9] Peng, T. C. and Pindroh, A. L., "An Improved Calculation of Gas Properties at High Temperature," Tech. Rep. D2-11722, Boeing Aiplane Co., 1962.

[10] Eric W. Lemmon, Richard T. Jacobsen, S. G. P. D. G. F., "Thermodynamic Properties of Air and Mixtures of Nitrogen, Argon, and Oxygen From 60 to 2000 K at Pressures to 2000 MPa," *J. Phys. Chem.*, Vol. 29, 2000, pp. 331–385.

[11] W., C. and Brinkley, K. L. S., "Chemical Equilibrium of Ablation Materials Including Condensed Species," Tech. rep., NASA, 1969.

[12] Shigeru KUCHI-ISHI, Shigeya WATANABE, S. U. H. T. T. K. K. S. and ITOH, K., "Comperative Force/Heat Flux Measurements Between JAXA Hypersonic Test Facilities Using Standard Model HB-2 (Part 2: High Enthalpy Shock Tunnel Results," Tech. rep., JAXA Research and Development Report, 2006.

[13] Scalabrin, L. C., *Numerical Simulation of Weakly Ionized Hypersonic Flow Over Reentry Capsules*, Ph.D. thesis, University of Michigan, 2007.

[14] S. Tissera, V. T. and Drikakis, D., "Real Gas Hypersonic Flow modeling using high order methods," *Journal os Spacecrafts and rockets*, Vol. 92, 2010, pp. –.

[15] O. Joseph, J. Michael Wright, L. S. G. H. H., "Computational Modeling of T5 Laminar and Turbulent Heating Data on Blunt Cones, Part 1: Titan Applications," *AIAA 2005-176*, 2005.

[16] Holden, M. and Wadhams, T., "Code validation study of laminar shock/boundary layer and shock/shock interaction hypersonic flow part a: Experimental measurements," *Tech. Rep. AIAA 2001-1031*, 2001.

[17] Holden, M. and Wadhams, T., "A review of experimental studies for dsmc and navierstokes code validation in laminar regions of shock/shock and shock/boundary layer interaction including real gas effects in hypervelocity flows," *AIAA-2003-3641*, 2006.